

Article

# Mechanisms and Dynamics of Layered Structure Formation During Co-Deposition of Binary Compound Thin Films

Gediminas Kairaitis \* and Arvidas Galdikas

Physics Department, Kaunas University of Technology, 50 Studentų st., LT-51368 Kaunas, Lithuania; arvidas.galdikas@ktu.lt

\* Correspondence: gediminas.kairaitis@ktu.lt

Received: 28 November 2019; Accepted: 25 December 2019; Published: 28 December 2019



**Abstract:** In the present paper, the formation of columnar and layered structure during co-deposition of binary thin films is analyzed by kinetic modeling. The kinetic model is based on phase field theory and involves the main processes taking place during binary film growth: adsorption, phase separation, Gibbsian surface segregation, surface and bulk diffusion. The process of phase separation is defined by the Cahn–Hilliard equation, which describes well the kinetics of formation of nanoparticles in binary system with a limited solubility of components. The formation of columns and layers can occur only if other processes such as diffusion and segregation take place. In this paper, the most attention is paid to the formation of multilayered structures during binary components co-deposition, which is experimentally observed, but whose mechanism of formation is not well understood. In the work presented, the mechanism of formation of layers is shown, and the conditions at which this mechanism starts to work are formulated. It is shown that very important aspects are surface segregation of one of the components and depth dependent diffusion.

**Keywords:** phase separation; surface segregation; kinetic modeling; thin films; multilayer

## 1. Introduction

Nanocomposite materials, due to their new unique and promising physical and chemical properties, have attracted much attention from the point of view of application as well as fundamental research because the processes which initiate self-organized modulation are not fully understood. A nanocomposite material is a multiphase solid material where one of the phases has either one, two or three dimensions of less than 100 nm, or the material includes structures with nanoscale repeat distances between the different phases [1]. Nanocomposite is not simply a structural variation at the nano- or mesoscales. The unique properties of nanocomposites come from the synergic interaction between the individual constituents, which plays an important role in enhancing or improving the functionalities [2]. The application of nanocomposites in surface engineering provides effective solution of many problems related to wear protection, hardness and/or toughness, biocompatibility, etc. [1]. Nanocomposites can be in the form of randomly or uniformly distributed nanoparticles, columns or layers [3]. Nanoparticles, columns or layers can be formed in various host materials such as different types of oxides, polymers or different allotropes of carbon [4]. Many experimental studies of this phenomenon can be found in literature. However, deep theoretical studies of mechanisms and dynamics of nanostructures formation are still insufficient, and mechanisms as well as dynamics of formations of nanocomposites are still not well understood. Several theoretical studies were devoted to the understanding of the growth mechanisms resulting in the formation of nanostructures in binary systems [5–14]. By the analysis of mechanisms leading to the formation of cylindrical columns made of

one component and surrounded by a phase made of another component during a binary films growth, it was shown [6,7] that the diameter of elongated domains depends on the ratio of adatom mobility over growth rate. A similar tendency was reported for the Al:Si thin films [8] grown by magnetron sputtering, where the diameters of the Al columns, embedded in a Si phase, were proportional to the surface diffusion length. The effects of stress and strain on the composition modulations seen during the growth of thin solid films by molecular-beam epitaxy are explored in [9]. It was shown that the elastic effects due to a difference between the elastic modulus of two components and crystal anisotropy modify the dynamical evolution and the steady state reached by the system. The results in Reference [10], where the influences of the surface diffusion, bulk diffusion and contents of film constituents on the phase structure of binary thin films were explored, indicate that the thin film phase structure depends on both, the ratio of the diffusion coefficient over the growth rate  $D_s/v$  and the concentrations of film constituents. Reference [11] shows that, depending on the metal content in the Ni:C thin films, the surface segregation of Ni can result in the formation of the columnar or layered patterns.

From the point of view of dynamic modelling and physical mechanisms of nanocomposite formation, the most incomprehensible is the layered structure (sandwiched) formation during simultaneous deposition of both components during binary films growth. Despite several models based on segregation proposed, catalytic action of metal, radiation enhanced diffusion, etc. [15,16], the origin of layering and its mechanism and dynamics are not fully understood. It was found experimentally that there is some minimum metal content required to form a layered structure [17,18]. In Reference [14], the phase diagram of morphological patterns proposed from the theoretical analysis reveals the dependence of various modulated microstructures (from layers to columns) on phase fraction and normalized deposition rate. It was shown in [5,12,14] that very important process for layered structure formation is spinodal decomposition, which induces the segregation and phase separation of components. In Reference [12], the growth of a spinodally unstable system evolving by the bulk diffusion was examined. It was shown that the spontaneous formation of a superlattice with layers parallel to the surface occurs when material is deposited at a composition unstable against spinodal decomposition at intermediate deposition rates. Reference [5] investigates the formation of alternating metal-rich and metal deficient layers in the Ti:C thin films. The effects of the growth rate and concentrations of Ti on the phase structure are investigated by a model based on the Cahn–Hilliard equation. It was shown that the formation of a structure containing alternating multilayers can be promoted using a relatively low growth rate. In Reference [13], it is shown that with increasing interdiffusion length as a result of increasing substrate temperature, the transition from layered to columnar and, finally, to random structures occurs.

From Refs. [5,12–14], two mechanisms of alternating layers formation can be distinguished. Refs. [5,12] consider the mechanism for spontaneous layering that is triggered by the interaction between the substrate and the deposited species. In Refs. [5,12] the substrate is assumed to favor the formation of a layer of one phase on the substrate, and those works clearly show that spinodal decomposition (under favorable growth conditions) can lead to the formation of a layered structure during continuous and simultaneous deposition of both components. From Refs. [5,12], one can deduce that the use of a relatively high value of the ratio of diffusion coefficient over growth rate promotes the formation of alternating layers. In Refs. [13,14], another mechanism for the formation of self-organized layers is proposed. The mechanism considered in [13,14] consists of two main stages. The first one is the formation of the chessboard like structure that initially develops in the top layers of a growing film. Later, the clusters made of same component connect to each other to form alternating layers. As shown in [13,14], the formation of multilayers can be obtained by using either a relatively low temperature [13] or a relatively high deposition rate [14] so that mechanism resulting in multilayers appears to be promoted by using a relatively low value of the ratio of diffusion coefficient over growth rate. The formation of alternating layers has been experimentally observed at various substrate temperatures, for example, at temperatures of 450 or 510 °C as shown in [15] and at room

temperature as shown by Refs. [18,19]. The models mentioned earlier fail to explain the formation of alternating layers at low substrate temperatures when no chessboard like structure formation is observed in initial growth stages. The chessboard like structure formation is not reported in [18,19].

This work is focused on the exploration of conditions which can result in the formation of structures containing self-assembled alternating layers. The basis of the previously published kinetic model [10,11], which includes such processes as adsorption, phase separation, surface segregation, surface and bulk diffusion, is used to model the growth and the formation of thin films. New function describing the free energy of a homogenous system is introduced. The influences of the surface and bulk diffusions, concentrations of thin film components, growth rate and surface segregation are investigated by using the modified model. The results of the modified and previous models are compared. The modeling results reveal that, depending on the parameters of the model such as diffusion coefficient, growth rate and contents of thin films components, the different growth modes resulting in the phase structures containing metal nanoparticles, nanocolumns or alternating metal-rich and metal-deficient layers can be obtained. The simulation results are compared with the experimental data.

## 2. Model

The model which considers the processes of phase separation, surface segregation and depth dependent bulk diffusion taking place during growth of binary carbon–metal films with a limited solubility of components was recently proposed in our previous works [10,11]. It was assumed that the limited solubility can lead to the phase separation and/or phenomena of Gibbsian surface segregation at elevated temperatures. For Gibbsian segregation, the two factors are responsible: (1) surface free energy (of surface tension) and (2) enthalpy (heat) of sublimation. The processes of phase separation and surface segregation are described by using the Cahn–Hilliard equation [20] with an additional term  $dg(\varphi)/d\varphi$  added [11], which describes the process of surface segregation

$$\frac{\partial \varphi}{\partial t} = \nabla D \nabla \left( \frac{df(\varphi)}{d\varphi} - \gamma \nabla^2 \varphi + \frac{dg(\varphi)}{d\varphi} \right), \quad (1)$$

where  $D$  is a diffusion coefficient,  $\gamma$  is a power coefficient of phase gradient. The function  $f(\varphi)$  is a potential of phase separation whose analytical form is very important for the mathematical description of process kinetics. It is known from the Landau formalism that for a symmetrical phase diagram ( $\varphi \in [-1, +1]$ ) it has a form containing only even powers of  $\varphi$ . The order of the function  $f(\varphi)$  determines the solubility of a binary system. The thermodynamically stable system is stable if the condition  $\partial^2 f(\varphi)/\partial \varphi^2 > 0$  is fulfilled and becomes unstable when this second derivative becomes negative. That is because in the composition with spinodal, a homogeneous solution is unstable against microscopic fluctuations [21,22]. Therefore, the inflection points  $\varphi_{\text{inf}}$  at  $\partial^2 f(\varphi_{\text{inf}})/\partial \varphi^2 = 0$ , define the solubilities of a system. For quite low solubilities the order of function must be quite high. From the conditions that function  $f(\varphi)$  must have minimums at points  $\varphi = \pm 1$  (these points denote phases of pure components, pure metal phase and pure host material phase): (1)  $\partial f(\pm 1)/\partial \varphi = 0$ , (2)  $\partial^2 f(\pm 1)/\partial \varphi^2 > 0$ , function  $f(\varphi)$  takes the following form:

$$f(\varphi) = 2(2\varphi^{10} - \varphi^8 - \varphi^6 - \varphi^4 - \varphi^2 + 2). \quad (2)$$

The term  $dg(\varphi)/d\varphi$  in Equation (1) is newly [11] included into the Cahn–Hilliard equation and denotes the surface free energy and describes the process of Gibbsian surface segregation.

$$dg(\varphi)/d\varphi = (W_A - W_B)/2, \quad (3)$$

where  $W_A, W_B$  are the surface energies of the pure components A and B. The surface energies define the atomic flux directions of segregating components. If  $W_A < W_B$  the segregating (to the surface

of a growing film) component is A, and a flux of component A atoms from the second layer to the surface layer takes place. The surface becomes enriched with component A. If  $W_A > W_B$ , everything is opposite, the segregating component is B, and a flux of component B atoms from the second layer to the surface layer takes place. The rate of this flux is directly proportional to the difference between surface free energies  $W_A - W_B$ . For deeper bulk layers it is assumed  $g = 0$ , this means that segregation takes place only at the surface, not in bulk layers. Normally, the Gibbsian surface segregation takes place at elevated temperatures (at high enough atom mobility), but it also can take place at lower temperatures under an external particle radiation (ions, electrons, photons), which enhances the mobility of surface atoms or during a deposition of energetic particles (during film growth).

In the systems where radiation enhanced diffusion initiated by an external irradiation of the surface by atomic particles can take place, the diffusion coefficient depends on the distance from the surface. For the dependence of the diffusion coefficient on depth, the hyperbolic tangent function is used [5]:

$$D_{i,j} = D_0 \left( 1 - \tanh^2 \left( \frac{h(i-1)}{l} \right) \right), i = \overline{1, N_1}, j = \overline{1, N_2} \quad (4)$$

where  $D_0$  is a value of the diffusion coefficient at the surface layer,  $h$  is the thickness of one monolayer, the parameter  $l$  is the dispersion parameter and defines the depth at which the value of the diffusion coefficient is 2.5 times lower compared to that at the surface;  $i$  is the layer number ( $i = 1$  denotes the surface layer).

Both diffusion and segregation are functions of temperature. Different diffusion coefficients for different temperatures are used in our calculations. For the dependence of diffusion coefficient on temperature the Arrhenius law is used. The surface segregation term  $g$  given by Equation (3) is independent on temperature, but the segregation process itself becomes dependent on temperature, because in Equation (1) there is a multiplication by temperature dependent diffusion coefficient as  $D \cdot \nabla (dg/d\varphi)$ .

The film growth is described through the adsorption process which is included into the model through the following equations [10,11] for surface  $i = 1$  and deeper layers  $i > 1$ :

$$\begin{aligned} \left( \frac{\partial \varphi_{1,j}}{\partial t} \right)_{ad} &= -k_{12}(1 - \varphi_{1,j})i_A + k_{21}(1 - \varphi_{1,j})i_B \\ \left( \frac{\partial \varphi_{i,j}}{\partial t} \right)_{ad} &= V_A^* (\varphi_{i-1,j} - \varphi_{1,j}), \end{aligned} \quad (5)$$

where,  $k_{nm}$  are the sticking coefficients of  $n$ -th type atoms (arriving at the surface) to the  $m$ -th type surface atom, and  $V_A^*$  is the film growth rate.

### 3. Results and Discussion

Figure 1 shows the calculated cross-sectional views of binary phase-separated thin films deposited at the different diffusion coefficients  $D_0$  and different film compositions. Areas of cross-sectional views made of pure phase A are colored in yellow, pure phase B is colored in blue. Component A is the component which segregates to the surface of a film. Depending on system, both metal [23,24] or carbon [15,16,23] may segregate to the surface. Component A is the host material, and in nanocomposites, the host material mostly is carbon. Therefore, in Figure 1, component A can be associated with carbon and component B with metal. Both components are co-deposited simultaneously with parallel fluxes during the whole growth process. In the calculations, the growth rate was kept at 4 nm/s, and the value of diffusion dispersion parameter  $l = 17$  nm was used. These calculations were performed at different diffusion coefficients  $D_0$  by changing the concentration of component B from 15 to 50 at%. The increase in the diffusion coefficient can be associated with an increase in temperature according to the Arrhenius law. At the low diffusion coefficient and the relatively low concentration of component B (at 15%), the tendency to form clustered structures is observed, which

transforms into the columnar structure with the increase in the content of component B (see top row of pictures from right to left in Figure 1). The carbon near the metal surface crystallizes in 2-d regime and forms graphene layers because metal surfaces may reconstruct providing epitaxial fits with the (0001) graphite face [25,26]. This leads to the growth of different kinds of carbon structures such as nanotubes [27] or diamond like carbon matrix [28,29] (through  $sp^2$  to  $sp^3$  C-C bond transition) detectable by Raman [30], X-ray photoelectron or Auger electron spectroscopy [29]. Considering carbon film growth structure, several aspects are important such as the existence of different kinds of internal stress, growth temperature, growth rates, energy transfer of arriving particles, the role of the chemical affinity of the substrate material, etc. [31]. The increase in the diffusion coefficient enhances the layering process (see pictures in the second and the third rows of Figure 1). The increase in concentration makes layers thicker (compare pictures at both edges in third row). However, the picture in the middle row of Figure 1 shows that with the continuous increase in the content of component B, the formation of layered and clustered structures alternates from layers to clusters and back. With the increase in the diffusion coefficient, this tendency of alternation decreases, and the growth of alternating layers is promoted (see third row pictures in Figure 1). The additional calculations show that the thickness of layers is highly influenced by the value of  $l$ . For example, when using 50% content of metal and  $D_0 = 2.2 \times 10^{-17} \text{ m}^2/\text{s}$ , the multilayered structures were formed for  $l \geq 15 \text{ nm}$ . The thickness of layers of about 25 nm was obtained at  $l = 15 \text{ nm}$ , whereas the increases in value of  $l$  up to 50 and 90 nm result in the increases in the thicknesses up to 38 and 40 nm, respectively. Therefore, the parameter  $l$  can be very important for the control of the thicknesses of alternating layers.

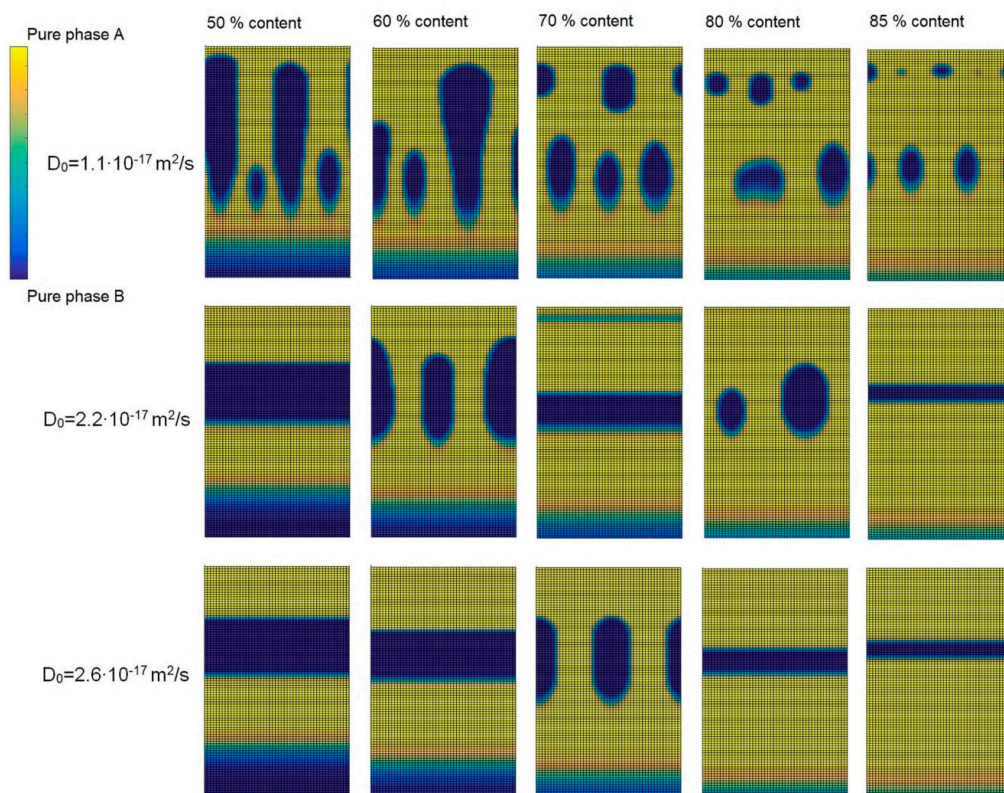


**Figure 1.** The calculated cross-sectional views of binary thin films at different diffusion coefficients and binary film compositions.

The dynamics of formation of the layered structure are analyzed by calculations presented in Figure 2, where the evolution of the thin film phase structure in the early growth stages and the formation of the second layer are shown. The calculations are performed at the film composition 40% of A and 60% at % of B, because the layered structure is more likely to be formed only at high enough

concentrations of both components [18]. From Figure 2a, pictures taken at film growth times  $t = 0.4$  s and 0.8 s (units are relative), it is seen that in the early growth stages, the individual nanoparticles of segregating component A are formed. Due to the lower surface tension, component A tends to diffuse from bulk layers to the surface layer and accumulate at the surface of the growing film. Due to the accumulation of component A at the surface of the growing film, the dimensions of nanoparticles made of pure phase A steadily increase. Nanoparticles start to coalesce at  $t = 1.2$  s. As a result, the formation of the layer made of pure phase A lying on the top takes place (see Figure 2a at  $t = 2$  s). In later growth stages, both initial layers of phase A and phase B grow thicker (Figure 2a  $t = 6$ –14 s), because particles of component B, adsorbed on the surface of the growing film, diffuse through the layer of phase A and stick to the layer of phase B. Therefore, there was the explanation for the first layer formation on the top of the surface. The main reason for the surface layer formation is the surface segregation of component A. However, there are still open question about the mechanism and dynamics of formation of the second layer of phase A.

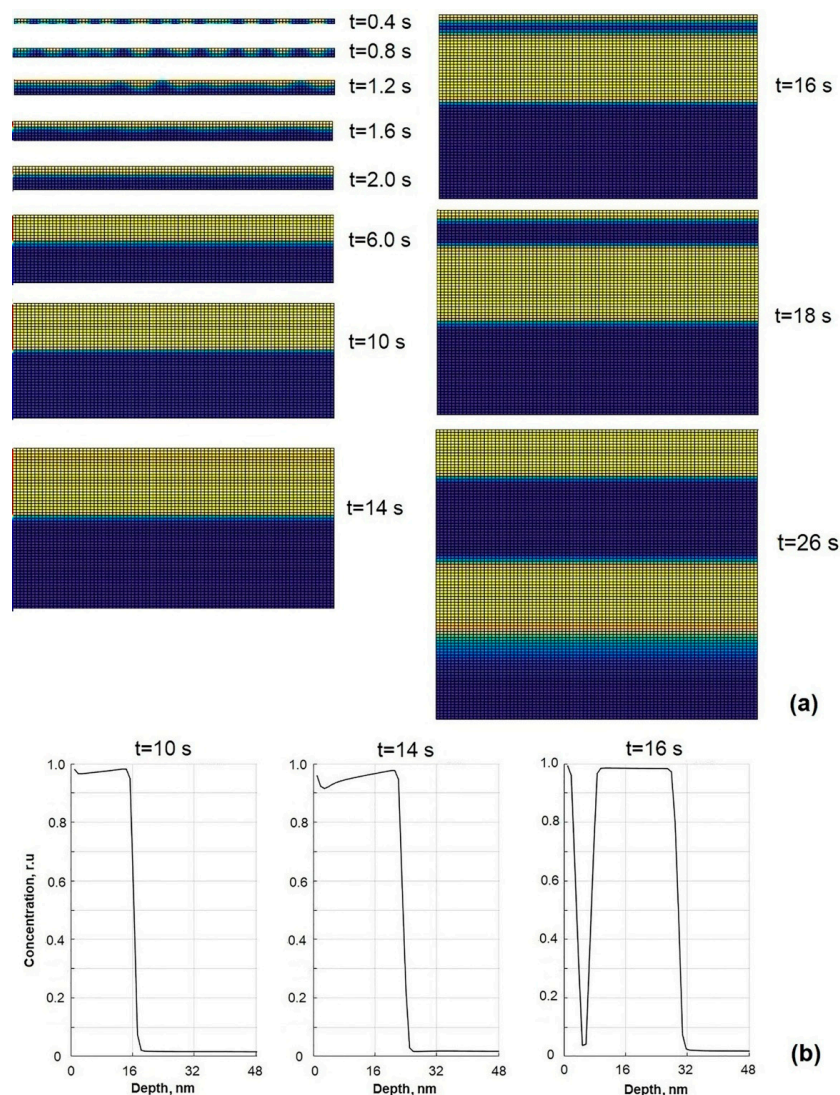


**Figure 2.** The dynamics of binary thin film phase structure in the early growth stages: (a) cross-sectional views and (b) depth profiles of component A (yellow) at different moments of time showing the splitting of first layer into two new layers.

In Figure 2b, the depth profiles of component A at three different moments of time are presented. Those profiles show the dynamics how the top layer of phase A starts to split into two separate layers

with the layer made of phase B in the middle. Profiles in Figure 2b show the mechanism and dynamics of sandwiched structure formation. As it was noted before, segregating component A dominates at the surface of the growing film in all profiles. The local minimums (the concentrations are normalized as  $c_B = 1 - c_A$ ) near the surface in the depth profile curves show the position of the local maximums of concentrations of component B just below the surface because those atoms (of type B) already cannot reach the layer of phase B, which becomes too deeply located, and it is more favorable for the system to form a new cluster or layer. With the further film growth, the concentration of component B below the surface increases. That is seen from the heights of minimums in the depth profiles which increase with time (see Figure 2b at  $t = 10$  and  $14$  s). With a continuous increase in the amount of component B below the surface, finally, the layer of phase A splits into two separate layers (see Figure 2a,b) at  $t = 16$  s). One part of the layer of phase A remains on the surface, the second one appears deeper in the bulk of the film and moves away from the surface during the film growth as the thickness of the layer B between them increases. This process repeats periodically, and the formation of the third, fourth and higher layers takes place, like it is shown in Figure 3 and will be discussed below. Therefore, the new layer forms on the surface after splitting and separating the surface layer of the segregating component. As it follows from this discussion, for layered or sandwiched structure formation, several conditions must be fulfilled: (1) components must have low solubility, i.e., the system with well-expressed phase separation; (2) relative concentrations of both components must be quite high, tens of percent; (3) system must have significant surface segregation (Gibbsian or induced by external radiation or chemically [32]).

Talking quantitatively, it must be noted that at  $t = 14$ s (see Figure 2), the concentration of component B reaches the value of 8.5% at the depth of 2 nm. That value is greater than the solubility of component B in matrix of A. The solubility determined by Equation (2) is about 7.9 at %. Therefore, the formation of separate phase B below the surface of the growing film becomes energetically favorable. In our previous work [11] the function in form Equation (2) was adapted for the Ni:C system. Therefore, the calculations presented in Figure 2 also can be assumed as modelling of the Ni:C system and compared with experimental results presented in Reference [18] (see picture Figure 3 of Reference [18]). In these experimental results, the layered structure in the Ni:C film was obtained at room temperature and at the Ni content of 40%. Low temperatures (meaning low diffusivity) and high concentrations of both components as a necessary condition for layering were also reported in References [13,14].

In Figure 3, the dynamics of the formation of the third layer are analyzed (the formation of subsequent layers is analogous). At  $t = 26$  s (see corresponding picture in Figure 3), the two layers of phase A are still observed (B as well), but the depth profile shown on the right side of that picture shows a small minimum in the concentration curve of component A. This means that component B starts to accumulate below the surface because the layer of phase B (existing in the bulk) now is too deep to diffuse there. At  $t = 28$  s, this minimum becomes better expressed; the concentration of B at the depth of 2 nm is about 18%, which is higher than solubility 7.9 at %, so at that moment of time, the formation of the layer made of component B was in progress. Finally, at  $t = 30$  s layer of component A splits into two layers with the layer of component B in the middle. Therefore, this process repeats forming layered or sandwiched binary film structures.

The above considered model with the potential of phase separation function given by Equation (2) explains very well the mechanism and dynamics of layered structure formation during simultaneous co-deposition and growth of binary films. However, there is still too early to compare the model results with experimental observations. In Ref. [18], it is reported that the  $\text{Ni}_3\text{C}$  compound nanoparticles are formed at the temperatures lower than  $300^\circ\text{C}$ . The formation of carbides is also reported in some other nanocomposites with self-organized layers [15,24]. This behavior needs to be incorporated into the model by including the possibility to form the carbide phase. We will consider the nickel carbide  $\text{Ni}_3\text{C}$  in order to compare our modeling results with experimental ones for the Ni:C films from Ref. [18]. In order to include the carbide phase, the new form of the potential of phase separation function  $f(\varphi)$  instead of Equation (2) must be found. Such a function must fulfill the following conditions: (1) in

interval  $[-1, 1]$ , the function  $f(\varphi)$  must have three minimum points at  $\varphi = -1$  (corresponding to the pure Ni phase), at  $\varphi = -0.5$  (corresponding to the  $\text{Ni}_3\text{C}$  phase), and at  $\varphi = 1$  (corresponding to the pure C phase) and also a local maximum point at  $\varphi = 0.25$ , which is assumed to be located in the middle between minimums at  $\varphi = -0.5$  and  $\varphi = 1$ . Such conditions cannot be fulfilled by any symmetric function (with respect to  $\varphi = 0$ ) given by Equation (2). The function must contain odd powers of  $\varphi$ . We found a function that fulfils the listed conditions. This function takes the following form:

$$f(\varphi) = c(a_1\varphi^8 + a_2\varphi^6 + a_3\varphi^5 + a_4\varphi^4 + a_5\varphi^3 + a_6\varphi^2 + a_7\varphi),$$

with

$$a_1 = 0.04234; a_2 = -0.101; a_3 = 0.0197; a_4 = 0.082;$$

$$a_5 = -0.03868; a_6 = -0.03016; a_7 = 0.0174;$$
(6)

where  $c$  is a parameter, whose value  $c = 100$  will be used in the calculations presented below. The plot of the function  $f(\varphi)$  in form of Equation (6) is given in Figure 4 (blue curve) together with the fragments of the second derivative (red lines). The amplitude of the second derivative is very high comparing with the amplitude of the function, which is why it is difficult to show both functions in one picture. However, the second derivative is very important because, as it was mentioned earlier, it determines the solubilities of components. The full curve of the second derivative (in red) together with the function (in blue) is shown in inclusion of Figure 4. The given values of parameters  $a_1, \dots, a_7$  ensures the existence of the mentioned extremums at the given particular points: minimums at  $\varphi = -1$ ,  $\varphi = -0.5$  and  $\varphi = 1$  and local maximum at  $\varphi = 0.25$ . The parameters  $a_1, \dots, a_7$  are fixed. Parameter  $c$  can be changed. Changes of parameter  $c$  do not affect the positions of the extremums. The difference between values of  $f(0.25)$  and  $f(1)$  and  $f(-0.5)$  (phases C and  $\text{Ni}_3\text{C}$ , respectively) is directly proportional to  $c$  so that difference can be controlled by changing the value of  $c$ . The new function  $f(\varphi)$  ensures that the formations of compositions corresponding to  $\text{Ni}_3\text{C}$  and C are favorable during the phase separation because of the deeper minimum points of the function  $f(\varphi)$  for those phases (this function directly related to the free energy) in comparison to the pure Ni phase at  $\varphi = -1$ . As it was discussed above, the points where the second derivative reaches zero value (corresponding to the inflection points of function  $f(\varphi)$ ) determine the solubilities of components. In Figure 4, we see that the second derivative of the function  $f(\varphi)$  reaches zero values four times in interval  $[-1, 1]$ , which means four different solubilities in the system. This is understandable, because now in the system we have three different pure phases of C, Ni and  $\text{Ni}_3\text{C}$ . These values, which are related to the solubilities, are indicated in Figure 4 as the positions of the inflection points of the function  $f(\varphi)$  in the  $\varphi$  axis. Because, the point  $\varphi = -1$  corresponds to the pure Ni phase and the point  $\varphi = 1$  (in the right side) represents the pure C phase, the solubilities of Ni are to the left of each minimum and the solubilities of C to the right of the minimums. The solubilities in terms of relative concentration can be recalculated by using the relation between concentration  $c$  and phase  $\varphi$ :  $c = (1 - |\varphi|)/2$ . Therefore, one can find the values of solubilities of different components defined by Equation (6): (1) The absolute value of  $(-1 - (-0.959))/2 \approx -0.0205$  corresponds to the solubility of C in the pure Ni; (2)  $(-0.5 - (-0.699))/2 \approx 0.0995$  is the solubility of Ni in the  $\text{Ni}_3\text{C}$  phase; (3) the absolute value of  $(-0.5 - (-0.163))/2 \approx -0.1685$  is the solubility of C in  $\text{Ni}_3\text{C}$  and (4)  $(1 - 0.844)/2 = 0.078$  is the solubility of Ni in the pure C phase. Note that in previous case, when the function  $f(\varphi)$  in form of Equation (2) was used, the solubilities of Ni in C or C in Ni were equal (function Equation (2) is symmetric), and the value of the solubility was 0.079; now it is 0.078.

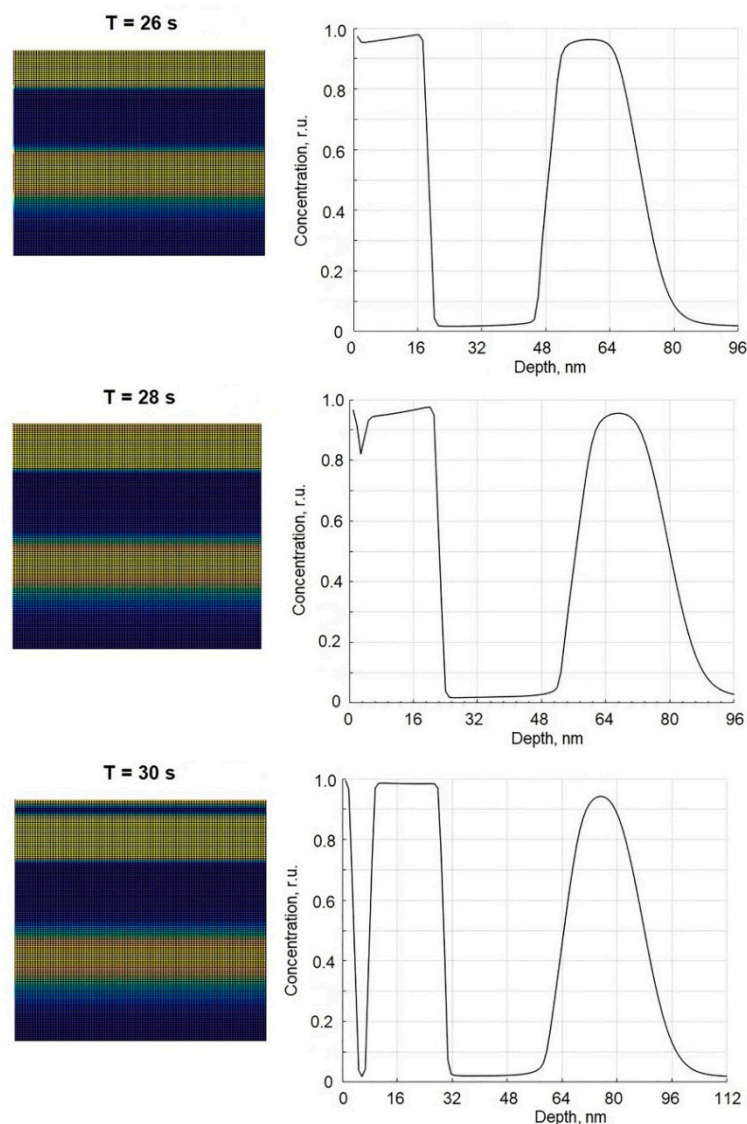


**Figure 3.** The kinetics of third layer formation: on the left the cross-section pictures of film structure at different moments of time and on the right the corresponding concentration profile of segregating component.

In further modeling, we will consider carbon to be the component that segregates to the surface during a film growth. We assume that the segregation of C is caused by the difference between the surface energies of metal phase (or metal carbide) with free incorporated carbon and pure carbon phase. The surface segregation of carbon has been experimentally observed in the C:Fe [23] and C:Cr [15] thin films, where the formations of the metal carbide phases were also reported. The experimental analysis of a layered structure formation in the C:Cr [15] films shows that the metal carbide layer adjacent to the substrate grows first. The growth of the first layer (adjacent to the substrate) is accompanied by the segregation of the excess amount of carbon (not incorporated in the metal carbides). This behavior of carbon was also observed during the growth of the C:Fe thin films [23].

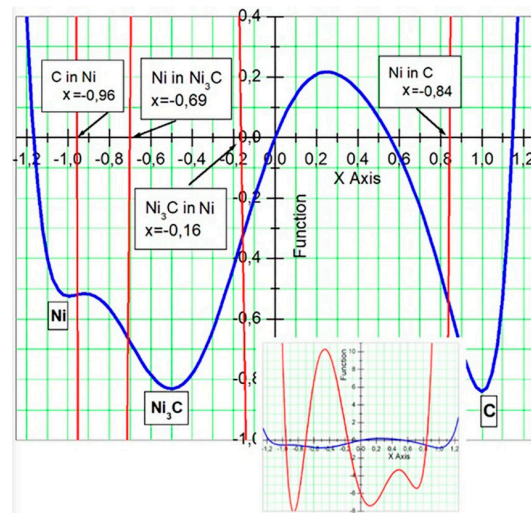


**Figure 4.** Plot of function  $f(\varphi)$  (blue line) Equation (6) and its second derivative (red line). Included are full curve of second derivative (red curve) of function  $f(\varphi)$  and function itself (blue curve). Three different phases, which correspond to three minimum points of function  $f(\varphi)$ , are shown. The solubilities of different phases, which related to the inflection points of function  $f(\varphi)$  or with zero values of second derivative, are indicated.

Figure 5 shows the calculated cross-sectional views of the binary thin films obtained by the modified model using the function  $f(\varphi)$  given by Equation (6) at different metal contents and different values of dispersion parameter  $l$  from Equation (4). All the other parameters were kept as constants. The Ni content was changed in the range from 15 to 40 at %. The value of  $D_0$  used in the calculations was  $4.35 \times 10^{-18} \text{ m}^2/\text{s}$  [18] and the film growth rate was 4 nm/s. C-rich regions are colored in yellow.  $\text{Ni}_3\text{C}$ -rich regions are colored in blue. The parameter  $l$  determines how fast values of the diffusion coefficient decrease with depth. The parameter  $l$  defines the depth at which the local diffusion coefficient is about 2.5 times lower than the diffusion coefficient at the surface layer  $D_0$ , so the values of the local diffusion coefficient decrease slower with depth when the value of  $l$  is higher. From Figure 5 it is seen that the use of the greater value of  $l$  promotes the formation of a structure containing alternating layers. The growth of self-organized alternating layers was observed for each metal content at  $l = 10 \text{ nm}$ . From Figure 5b, where the cross-sectional view calculated at  $l = 8 \text{ nm}$  is given, it is seen that for the Ni content of 40 at % the thin film consists of alternating  $\text{Ni}_3\text{C}$  and C layers. Figure 5d,f shows that the formation of  $\text{Ni}_3\text{C}$  nanoparticles surrounded by C phase is favorable when the metal content is reduced to 28 or 25 at %.

The obtained results agree with the experimental results presented in Figure 3b of Ref. [18]. Figure 5h reveals that the multilayered structure can be obtained again by reducing the metal content to 15 at %, but the multilayered structure shown in Figure 5h is different from that given in Figure 5b. For the film with the Ni content of 15 at % given in Figure 5h, the thin film consists of alternating Ni-rich and Ni-deficient layers. The phase separation into the pure  $\text{Ni}_3\text{C}$  and C phases is not observed in that case. From Figure 5g,h, it is seen that the similar structures are observed for both cases of the metal content of 15 at %. For the film with the Ni content of 15 at % given in Figure 5h, the Ni concentration varies from 10 to 20 at % in Ni-deficient and Ni-rich layers, respectively. The similar behavior (similar variation in the metal concentration with depth) is observed experimentally in the Pt-DLC thin films [19]. Figure 2b in Ref. [19] shows the TEM cross-sectional image, which confirms the formation of alternating layered structures in the Pt-DLC system. Figure 2d in Ref. [19] shows the AES depth profile of a Pt-DLC film, which confirms the formation of the structures with alternating layers having a lower and a higher metal concentration. Since for the snapshot with the Ni content of 15 at % there is no phase separation into pure  $\text{Ni}_3\text{C}$  and C phases, the formation of the structure with Ni-rich and Ni-deficient layers (observed in Figure 5g,h) should not be attributed to the existence of the

minimum of  $f(\varphi)$  at  $\varphi = -0.5$  (corresponds to the  $\text{Ni}_3\text{C}$  phase, Figure 4) but to the form of the function  $f(\varphi)$  in the interval  $[0.25, 1]$  (or to be more precise, in interval  $[0.6, 0.8]$  whose endpoints correspond to the metal concentrations of 10 and 20 at %), which is different from that of the previously used 10-th degree polynomial function (given in Equation (2)).

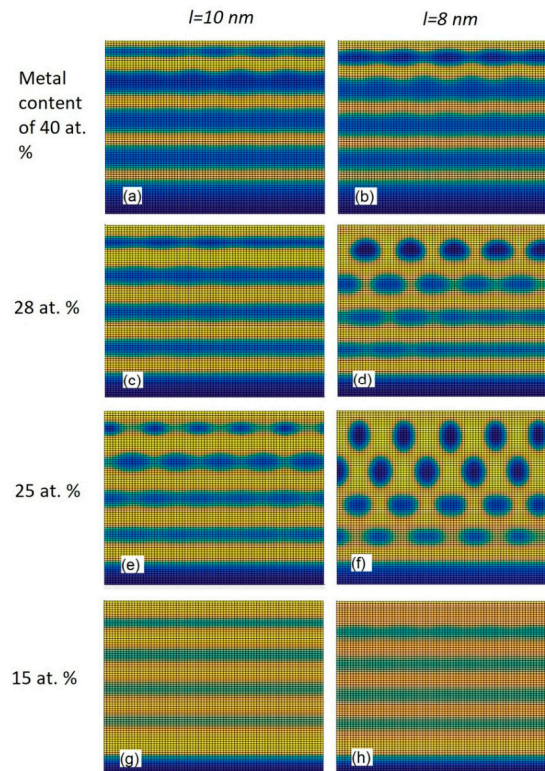


**Figure 5.** Snapshots obtained by using the modified model with different Ni contents and values of parameter  $l$ .

Since the given modeling experiments are compared to the experimental ones, performed at the relatively low substrate temperature, the values of diffusion coefficient  $D_0$  and growth rate used in the presented calculations (the initial values) are kept close to those that were used to model the phase structure at a relatively low substrate temperature in [11]. The difference between surface energies (used in the presented calculations) is kept the same as in [11]; the parameter  $l$  is varied in the range close to that used in [11] ( $l = 9$  and  $12$  nm used in [11]). The influences of the diffusion coefficient  $D_0$  and the growth rate on the phase structure will be later investigated by varying those parameters around the given initial values. It is important to note that the given results (calculated using  $D_0 = 4.35 \times 10^{-18}$  m<sup>2</sup>/s, the growth rate of 4 nm/s and the growth time of 20 s) can easily be linked to the experimental ones that may use, for example a different growth rate (from 4 nm/s). Since the units of the diffusion coefficient and the growth rate are m<sup>2</sup>/s and nm/s, respectively, the snapshots identical to those shown in Figure 5 can be obtained by using, for example,  $D_0 = 4.35 \times 10^{-19}$  m<sup>2</sup>/s (10 times lower than the original value), the growth rate of 0.4 nm/s (also 10 times lower than the original value) and the growth time of 200 s (10 times greater than the original value). Any other multiplier can be used to change the time scale in this way. Changes in the time scale do not affect the tendencies observed. Therefore, all the presented results can easily be linked to any other results that may use a different value of the growth rate (or diffusion coefficient).

Figure 6 shows a functional dependence of layer thicknesses versus metal content in film. The dependence was drawn from the data that are partially given in Figure 5a,c,e,g. From Figure 6, it is seen that the thickness of the metal-rich layer mostly increases as the metal content increases. The thickness of the metal-rich layer decreases when the metal content is changed from 15 to 25 at %

and then continuously increases with the further increase in the metal content. The thickness of the carbon-rich layer varies in an opposite way. From Figure 5e,g, it is seen that the final distribution of components in these two films is significantly different. For the film with the total metal content of 25 at %, the metal concentration varies from 5 to 55 at % in metal-deficient and metal-rich layers, respectively, whereas for the film with the metal content of 15 at %, the metal concentration varies from 10 to 20 at %. These variations in the metal concentrations in metal-rich and metal-deficient layers obtained by increasing the metal content from 15 to 25 at % explain the non-monotonous dependence of layer thicknesses on the metal content shown in Figure 6. Figure 5 reveals that the phase separation in the metal-carbon film can be intensified by increasing the metal content. Similar tendency was observed for the Cu:C films grown by pulsed filtered cathodic vacuum arc deposition [17], where the films with the different metal contents (Cu: 0–28 at %) were analyzed. From Figure 3 in [17], where the cross-section SEM images of samples with the Cu contents of 0–28 at % are presented, the formation of alternating multilayer seems to be enhanced by the Cu content.

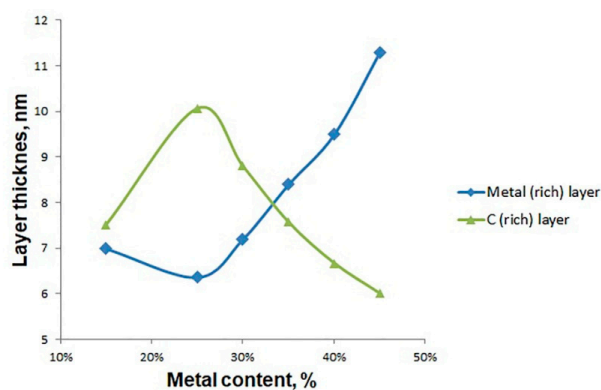


**Figure 6.** Dependencies of layer thickness on the metal content in layered thin films.

Figure 7 shows the cross-sectional views and depth profiles of carbon obtained by using the different diffusion coefficients  $D_0$  but with the constant Ni total content of 45 at % in the films. All the other parameters were kept as constants. The diffusion coefficient  $D_0$  was varied in the range from  $2.0 \times 10^{-18} \text{ m}^2/\text{s}$  to  $1.3 \times 10^{-17} \text{ m}^2/\text{s}$ . The growth rate was 4 nm/s. The value of diffusion dispersion parameter  $l = 10 \text{ nm}$  was used. From Figure 7, it is seen that various nanostructures can be produced by varying diffusion coefficient  $D_0$  (e.g., with temperature or external beam radiation). Figure 7e shows that the use of the highest diffusion coefficient  $D_0$  induces the formation of the columnar structure, which grows after the development of few metal-rich and metal-deficient layers in the early growth stages.

From Figure 7c,d, it is seen that the decrease in the diffusion coefficient  $D_0$  from  $1.3 \times 10^{-17}$  to  $8.5 \times 10^{-18}$  or  $4.1 \times 10^{-18} \text{ m}^2/\text{s}$  results in the formation of alternating layers. Besides, the thicknesses of metal-rich and carbon-rich layers shown in Figure 7d are visually greater than those given in Figure 7c, which indicates that the use of a higher diffusion coefficient  $D_0$  results in the greater thicknesses of layers. Figure 7b,c demonstrates that the further decrease in the diffusion coefficient  $D_0$  from  $4.1 \times 10^{-18}$  to  $3.0 \times 10^{-18} \text{ m}^2/\text{s}$  disrupts the formation of alternating layers, and the formation of individual clusters is favorable. Figure 7a shows that the structure containing alternating layers can be obtained again by reducing the diffusion coefficient  $D_0$  to  $2.0 \times 10^{-18} \text{ m}^2/\text{s}$ , but the composition of the thin film given in Figure 7a is different from those given in Figure 7c,d. In Figure 7a the concentration of the metal varies from 40 to 70 at % in metal-deficient and metal-rich layers (see depth profile), respectively, so there is 30% difference between the carbon concentrations in metal-rich and metal-deficient layers. For the films shown in Figure 7c,d, differences are 45 and 55 at % on average, respectively, so the increase in the diffusion coefficient  $D_0$  enhances the pureness of alternating layers. From Figure 7d,e, it is seen that the change from a structure containing alternating layers to a columnar structure can be obtained by increasing the value of diffusion coefficient. This tendency agrees with the findings

from References [18,19,23,33–35]. Works [19,23] indicate that the structures containing metal-rich and metal-deficient alternating layers had been produced without any additional heating (at room temperature) in Pt:C [19], Ni:C [19], Cu:C [19], Au:C [23], Fe:C [23] thin films. Ref. [18] also shows that the multilayer structure can be obtained at room temperature, whereas an increase in the substrate temperature results in the formation of a columnar structure. A study of the C:Ni thin films grown by ion beam co-sputtering presented in [33] reveals the formation of Ni nanocolumns surrounded by a carbon phase at 300 °C. Another study of the C:Ni thin films deposited by DC magnetron sputtering [34] shows the formation of a columnar structure made of Ni grains embedded in a matrix consisting of an amorphous and/or graphite-like carbon below 400 °C. The study of the Fe:C thin films grown by ion-beam sputtering co-deposition [35] reports the formation of Fe nanocolumns surrounded by a carbon phase at 300 °C. If we assume that an increase in the substrate temperature results in an increase in the diffusion coefficient  $D_0$ , our modified model can explain the transition from a multilayer structure to a columnar structure by increasing substrate temperature. In Reference [15], where the C:Cr thin films were investigated, it is shown that the formation of self-organized alternating layers can be achieved by using the particular substrate temperatures and the bias voltages (see Figure 3 in Ref. [15]); the use of higher or lower values of those parameters does not lead to the growth of alternating layers. This behavior can be seen in Figure 7, where only one parameter  $D_0$  was varied.

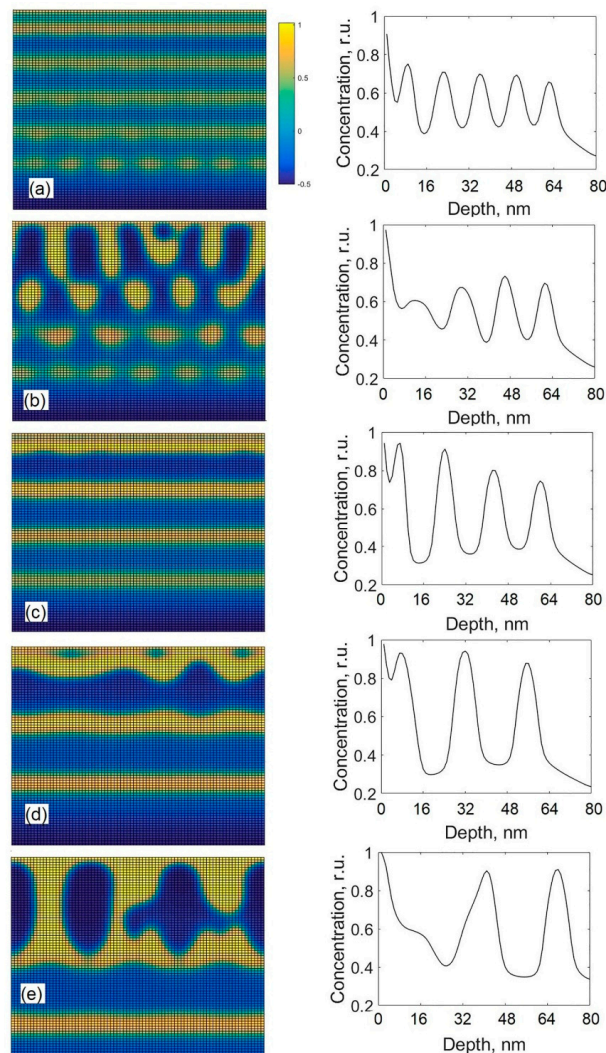


**Figure 7.** Cross-sectional views and depth profiles of carbon obtained by the modified model using different diffusion coefficients:  $2.0 \times 10^{-18} \text{ m}^2/\text{s}$  (a),  $3.0 \times 10^{-18} \text{ m}^2/\text{s}$  (b),  $4.1 \times 10^{-18} \text{ m}^2/\text{s}$  (c),  $8.5 \times 10^{-18} \text{ m}^2/\text{s}$  (d),  $1.3 \times 10^{-17} \text{ m}^2/\text{s}$  (e).

Previously, it was observed that the film growth rate significantly influences the structure of nanocomposites. Figure 8 shows the cross-sectional views and depth profiles of carbon obtained using different film growth rates (parameters  $V_A^*$  in Equation (5)). The growth rate varies in the range from 2 to 8 nm/s. The value of  $D_0$  used in the calculations was  $4.1 \times 10^{-18}$  m<sup>2</sup>/s (the same as for Figure 7c, i.e., the case with well-expressed layers). All the other parameters were kept the same as previously stated. From Figure 8, it is seen that the multilayer structures were grown by using the growth rates of 2, 4, 8 nm/s, but at the highest rate of 8 nm/s, the depth distribution of thin film components are different from the ones obtained using the lower rates. From the depth profile, given in Figure 8, it is seen that the growth rate of 8 nm/s hinders the separation into pure phases, whereas the phase separation into the purer phases is observed at the rates of 2 and 4 nm/s. At the growth rates of 5 or 6 nm/s, the structures containing individual nanoparticles of various shapes are produced. Similar dependences of the phase structure on the growth rate are reported in the other theoretical works [12,13]. In Ref. [12], it is shown that the thicknesses of alternating layers can be increased by decreasing the growth rate, which agrees with our calculations given in Figure 8 (rates of 2 and 4 nm/s). In Ref. [13], it is shown that the change of the phase structure from a multilayered structure to that containing individual elongated nanoparticles can be obtained by increasing substrate temperature. This behavior can be seen in Figure 7. From Figures 7 and 8, it is seen that the decrease in the film growth rate and the increase in the diffusion coefficient result in the similar effect on the phase structure, which suggests that the evolution of the phase structure is influenced by the ratio of  $D_0$  over growth rate.

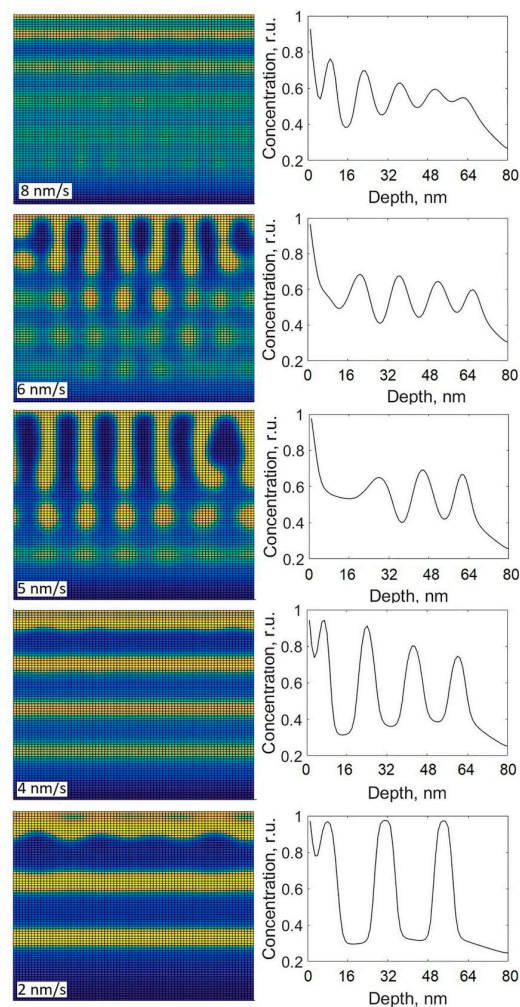


**Figure 8.** Cross-sectional views and depth profiles of carbon obtained by the modified model using different growth rates.

The influence of the surface segregation is shown in Figure 9 where the cross-sectional views and the depth profiles of carbon calculated at different values of the difference  $W_a - W_b$  are presented. The difference  $W_a - W_b$  denotes the difference between the surface energies of metal carbide phase and pure carbon phase. The surface segregation flux (to the surface layer from the bulk) is directly proportional to that difference. Results presented in Figure 9a,b were calculated using  $W_a - W_b = 4.8 \times 10^8 \text{ J/m}^3$ . Results in Figure 9c,d were calculated using  $W_a - W_b = 9.6 \times 10^8 \text{ J/m}^3$ , which was used in all the calculations presented earlier. The other model parameters were as follows:  $D_0 = 3.5 \times 10^{-18} \text{ m}^2/\text{s}$ ,  $l = 10 \text{ nm}$ . From Figure 9, it is seen that the formation of alternating layers is obtained by using the greater value of  $W_a - W_b$ , whereas the use of the lower value of  $W_a - W_b$  favors the growth of a columnar structure and, for depths greater than 8 nm, an almost uniform depth distribution of the segregating component is observed (see Figure 9b). In the given case, the use of the lower value of  $W_a - W_b$  promotes the lateral phase separation, which results in the formation of a columnar structure (if diffusion coefficient  $D_0$  is great enough). These results also show that the surface segregation can hinder the lateral phase separation, and this process can be important for the formation of a multilayered structure.

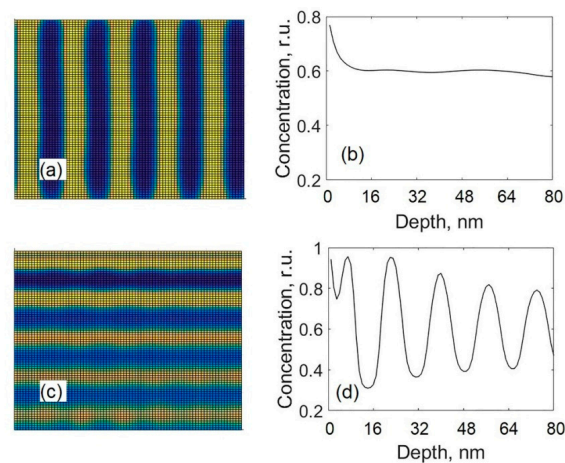


**Figure 9.** Cross-sectional views and depth profiles of carbon obtained with different values of  $W_a - W_b$ :  $W_a - W_b = 4.8 \times 10^8 \text{ J/m}^3$  (a,b);  $W_a - W_b = 9.6 \times 10^8 \text{ J/m}^3$  (c,d).

The surface segregation used in our model is not the only way to induce the development of alternating layers. Another factor such as a larger affinity of the substrate to one of the components [5] can promote the development of multilayers, but the formation of alternating layers influenced by that larger affinity can be interrupted in later growth stages, though the growth of alternating layers was observed in initial growth stages.

The several growth modes resulting in the development of different phase structures can be distinguished from Figures 5 and 7–9. When  $D_0$  is relatively high, the lateral phase separation is promoted, and the growth of a columnar structure through the surface diffusion is favorable. In this case, the pure phases of each component (corresponding to the minimums of  $f(\varphi)$ ) are produced. A decrease in diffusion coefficient  $D_0$  slows the process of phase separation down, and both components fail to separate in pure phases before being covered by subsequent layers. In this case, the phase separation into pure components near the surface of the growing film and the formation of a columnar structure are disrupted. In this situation, the phase separation can occur through the bulk diffusion. The phase separation through the bulk diffusion can result in the separation into pure phases if the diffusion coefficients within the bulk are high enough. This occurs not only during nanocomposite formation through the co-deposition of binary films but also may occur during post deposition processes, e.g., laser annealing when nanoparticles are formed [36]. Depending on the values of the diffusion coefficient, the contents of thin films components and surface segregation rate, multilayered structures and the patterns containing individual nanoparticles can be produced. High metal content

and/or high segregation rate promote the development of alternating multilayers. Further decrease in diffusion coefficient  $D_0$  hinders the separation into pure phases even within the bulk, and alternating metal-rich and metal-deficient layers of a relatively low pureness can be obtained. As shown by Figures 5 and 8, similar changes in the phase structure can be induced by varying the growth rate and the concentrations of thin films components. An increase in the growth rate results in a similar effect as the decrease in  $D_0$ . From Figures 7–9, one can deduce that the formation of alternating layers occurs through the same mechanism that was revealed earlier by analyzing the formation of multilayers using the previous model (based on the symmetric function  $f(\varphi)$  Equation (2)). In all cases presented in Figures 7–9, the formation of new layers occurs through dividing the top layer of the segregating (to the surface) component into two layers. One of those layers always exists on the surface of the growing film; the second layer appears deeper in the bulk. The layer rich in non-segregating component is formed between those two layers. The main difference between our previous and modified models is that only the formation of pure component alternating layers can be reproduced by the previous model (based on the symmetric function  $f(\varphi)$  Equation (2)). Therefore, in the system described by the previous model, only a relatively high diffusion coefficient (or a relatively high value of the ratio of diffusion coefficient over growth rate) ensures the formation of alternating layers. The modified model does not necessarily require a high diffusion coefficient for the formation of multilayers. Therefore, our modified model can explain the formation of alternating multilayers at relatively low temperatures. The modified model can also reproduce the growth of alternating layers of various levels of pureness. It is important to note that the formation of alternating metal-rich and metal-deficient layers of a desired pureness can be caused by the particular growth conditions (relatively lower content of metal, relatively higher growth rate and/or relatively lower value of  $D_0$  result in a lower pureness of layers) and the favorable form of function  $f$  (function curvature) in intervals whose endpoints correspond to the desired metal concentrations in metal rich and metal deficient layers. Those growth and thermodynamic conditions must be met simultaneously to get a desired multilayered structure.

#### 4. Conclusions

The conditions promoting the formation of self-organized alternating layers during a metal-carbon film growth have been analyzed by using two modifications of the model (symmetric and non-symmetric functions describing the free energy of a homogenous system were used). The mechanism of the growth of alternating layers has been revealed. The numerical calculations showed that the diffusion coefficient at the surface of a growing film and within the bulk (parameter  $l$ ), the growth rate, the concentrations of thin film constituents and the surface segregation rate were the important factors determining the phase structure of the thin films.

The analysis of the model using the symmetric function of the free energy of a homogenous system showed that the relatively high values of  $D_0$  and  $l$  ( $l$  must be higher than 15 nm in the given case) were the main factors promoting the growth of self-organized alternating layers. For a suitable combination of  $D_0$  and  $l$ , the growth of multilayers was observed at various thin film compositions; besides, the value of  $D_0$  seemed to influence the intervals of the contents of both components in which the growth of multilayers could be achieved.

The analysis of the model using the non-symmetric function showed that the relatively high value of diffusion coefficient (at the surface of a growing film)  $D_0$  induced the lateral phase separation, which resulted in the formation of a columnar structure. The change from a columnar structure to the one containing alternating layers can be obtained by reducing the value of  $D_0$ . Further decrease in  $D_0$  (as well as decrease in the metal content) may result in the formation of alternating layers of a relatively low pureness; this behavior cannot be reproduced by using the symmetric function. The model with the symmetric function requires a relatively high value of  $D_0$  to achieve the growth of self-organized multilayers and cannot reproduce the formation of alternating layers of a relatively low pureness. The increase in the growth rate induces a similar effect on the phase structure as the decrease in

$D_0$ . Relatively high values of metal content, segregation rate and characteristic length  $l$  promote the development of alternating layers.

If we assume that an increase in the substrate temperature results in an increase in the diffusion coefficient  $D_0$ , the modeling results obtained by using the non-symmetric function are consistent with experimental data where alternating layers were obtained at the relatively low substrate temperatures in C:Ni, Pt:C, Cu:C, Fe:C thin films, whereas the formation of the columnar structures were reported in C:Ni, C:Fe thin films grown at the higher temperatures.

**Author Contributions:** Conceptualization, G.K. and A.G.; methodology, G.K. and A.G.; software, G.K.; validation, G.K. and A.G.; investigation, G.K. and A.G.; writing—original draft preparation, G.K. and A.G.; writing—review and editing, G.K. and A.G.; visualization, G.K. and A.G.; supervision, A.G.; funding acquisition, G.K. and A.G. All authors have read and agreed to the published version of the manuscript.

**Funding:** This project has received funding from European Regional Development Fund (project No. 01.2.2-LMT-K-718-01-0071) under grant agreement with the Research Council of Lithuania (LMTLT), Vilnius, Lithuania.

**Acknowledgments:** Authors would like to express their gratitude for the following individuals for their expertise and contribution to the manuscript: Giedrius Laukaitis, Teresa Moskaliuviene, Kristina Bočkute.

**Conflicts of Interest:** The authors declare no conflict of interest.

## References

1. Tamulevičius, S.; Meškiniš, Š.; Tamulevičius, T.; Rubahn, H.G. Diamond like carbon nanocomposites with embedded metallic nanoparticles. *Reports Prog. Phys.* **2018**. [[CrossRef](#)] [[PubMed](#)]
2. Nan, C.-W.; Jia, Q. Obtaining ultimate functionalities in nanocomposites: Design, control, and fabrication. *MRS Bull.* **2015**, *40*, 719–724. [[CrossRef](#)]
3. Calderon Velasco, S.; Cavaleiro, A.; Carvalho, S. Functional properties of ceramic-Ag nanocomposite coatings produced by magnetron sputtering. *Prog. Mater. Sci.* **2016**, *84*, 158–191. [[CrossRef](#)]
4. Armelao, L.; Barreca, D.; Bottaro, G.; Gasparotto, A.; Gross, S.; Maragno, C.; Tondello, E. Recent trends on nanocomposites based on Cu, Ag and Au clusters: A closer look. *Coord. Chem. Rev.* **2006**, *250*, 1294–1314. [[CrossRef](#)]
5. Corbella, C.; Echebarria, B.; Ramírez-Piscina, L.; Pascual, E.; Andújar, J.L.; Bertran, E. Spontaneous formation of nanometric multilayers of metal-carbon films by up-hill diffusion during growth. *Appl. Phys. Lett.* **2005**, *87*, 213117. [[CrossRef](#)]
6. Atzmon, M.; Kessler, D.A.; Srolovitz, D.J. Phase separation during film growth. *J. Appl. Phys.* **1992**, *72*, 442–446. [[CrossRef](#)]
7. Adams, C.D.; Srolovitz, D.J.; Atzmon, M. Monte Carlo simulation of phase separation during thin-film codeposition. *J. Appl. Phys.* **1993**, *74*, 1707–1715. [[CrossRef](#)]
8. Fukutani, K.; Tanji, K.; Saito, T.; Den, T. Phase-separated Al-Si thin films. *J. Appl. Phys.* **2005**, *98*, 033507. [[CrossRef](#)]
9. Léonard, F.; Desai, R.C. Elastic effects and phase segregation during the growth of thin alloy layers by molecular-beam epitaxy. *Phys. Rev. B* **1997**, *56*, 4955–4965. [[CrossRef](#)]
10. Kairaitis, G.; Galdikas, A. Phase separation during thin film deposition. *Comput. Mater. Sci.* **2014**, *91*, 68–74. [[CrossRef](#)]
11. Kairaitis, G.; Grigaliūnas, A.; Baginskas, A.; Galdikas, A. Kinetic modeling of phase separation and surface segregation in growing a-C:Ni thin films. *Surf. Coat. Technol.* **2018**, *352*, 120–127. [[CrossRef](#)]
12. Daruka, I.; Tersoff, J. Self-assembled superlattice by spinodal decomposition during growth. *Phys. Rev. Lett.* **2005**. [[CrossRef](#)] [[PubMed](#)]
13. Derby, B.; Cui, Y.; Baldwin, J.K.; Misra, A. Effects of substrate temperature and deposition rate on the phase separated morphology of co-sputtered, Cu-Mo thin films. *Thin Solid Films* **2018**, *647*, 50–56. [[CrossRef](#)]
14. Lu, Y.; Wang, C.; Gao, Y.; Shi, R.; Liu, X.; Wang, Y. Microstructure map for self-organized phase separation during film deposition. *Phys. Rev. Lett.* **2012**. [[CrossRef](#)] [[PubMed](#)]
15. Hovsepian, P.E.; Kok, Y.N.; Ehasarian, A.P.; Haasch, R.; Wen, J.G.; Petrov, I. Phase separation and formation of the self-organised layered nanostructure in C/Cr coatings in conditions of high ion irradiation. *Surf. Coat. Technol.* **2005**, *200*, 1572–1579. [[CrossRef](#)]

16. Jurkevičiūtė, A.; Lazauskas, A.; Tamulevičius, T.; Vasiliauskas, A.; Peckus, D.; Meškiniš, Š.; Tamulevičius, S. Structure and density profile of diamond-like carbon films containing copper: Study by X-ray reflectivity, transmission electron microscopy, and spectroscopic ellipsometry. *Thin Solid Films* **2017**, *630*, 48–58. [[CrossRef](#)]
17. Pardo, A.; Buijnsters, J.G.; Endrino, J.L.; Gómez-Aleixandre, C.; Abrasonis, G.; Bonet, R.; Caro, J. Effect of the metal concentration on the structural, mechanical and tribological properties of self-organized a-C:Cu hard nanocomposite coatings. *Appl. Surf. Sci.* **2013**, *280*, 791–798. [[CrossRef](#)]
18. Abrasonis, G.; Kovács, G.J.; Ryves, L.; Krause, M.; Mücklich, A.; Munnik, F.; Oates, T.W.H.; Bilek, M.M.M. Möller, W. Phase separation in carbon-nickel films during hyperthermal ion deposition. *J. Appl. Phys.* **2009**, *105*, 083518. [[CrossRef](#)]
19. Wu, W.Y.; Ting, J.M. Growth and characteristics of metal-containing diamond-like carbon using a self-assembled process. *Carbon* **2006**, *44*, 1210–1217. [[CrossRef](#)]
20. Cahn, J.W.; Hilliard, J.E. Free energy of a nonuniform system. I. Interfacial free energy. *J. Chem. Phys.* **1958**, *28*, 258–267. [[CrossRef](#)]
21. Favvas, E.P.; Mitropoulos, A.C. What is spinodal decomposition? *J. Eng. Sci. Technol. Rev.* **2008**, *1*, 25–27. [[CrossRef](#)]
22. Bray, A.J. Theory of phase-ordering kinetics. *Adv. Phys.* **1994**, *43*, 357–459. [[CrossRef](#)]
23. Gerhards, I.; Stillrich, H.; Ronning, C.; Hofsaess, H.; Seibt, M. Self-organized nanoscale multilayer growth in hyperthermal ion deposition. *Phys. Rev. B* **2004**, *70*, 245418. [[CrossRef](#)]
24. Gerhards, I.; Ronning, C.; Vetter, U.; Hofsaess, H.; Gibhardt, H.; Eckold, G.; Li, Q.; Lee, S.T.; Huang, Y.L.; Seibt, M. Ion beam synthesis of amorphous carbon thin films containing metallic nanoclusters. *Surf. Coat. Technol.* **2002**, *158–159*, 114–119. [[CrossRef](#)]
25. Baraton, L.; He, Z.B.; Lee, C.S.; Cojocar, C.S.; Chtelet, M.; Maurice, J.L.; Lee, Y.H.; Pribat, D. On the mechanisms of precipitation of graphene on nickel thin films. *EPL* **2011**, *96*, 46003. [[CrossRef](#)]
26. Yang, J.; Chen, P. Mechanism of carbon filament growth on metal catalysts. *J. Catal.* **1989**, *115*, 52–64. [[CrossRef](#)]
27. Jin, L.; Zhao, X.; Qian, X.; Dong, M. Nickel nanoparticles encapsulated in porous carbon and carbon nanotube hybrids from bimetallic metal-organic-frameworks for highly efficient adsorption of dyes. *J. Colloid Interface Sci.* **2018**, *509*, 245–253. [[CrossRef](#)]
28. Galdikas, A.; Logothetidis, S.; Patsalas, P.; Gioti, M.; Pranevicius, L. The kinetics of sputtered deposited carbon on silicon: A phenomenological model. *Diam. Relat. Mater.* **2002**, *8*, 490–494. [[CrossRef](#)]
29. Neuville, S. Quantum electronic mechanisms of atomic rearrangements during growth of hard carbon films. *Surf. Coat. Technol.* **2011**, *206*, 703–726. [[CrossRef](#)]
30. Neuville, S. *Refined Raman Spectroscopy Fundamentals for Improved Carbon Material Engineering*; LAP LAMBERT Academic Publishing: Saarbrücken, Germany, 2014.
31. Neuville, S.; Matthews, A. A perspective on the optimisation of hard carbon and related coatings for engineering applications. *Thin Solid Films* **2007**, *515*, 6619–6653. [[CrossRef](#)]
32. Galdikas, A.; Pranevicius, L. *Interaction of Ions with Condensed Matter*; Nova Science Publishers: Huntington, WV, USA, 2000.
33. Abrasonis, G.; Krause, M.; Mücklich, A.; Sedláčková, K.; Radnóczy, G.; Kreissig, U.; Kolitsch, A.; Möller, W. Growth regimes and metal enhanced 6-fold ring clustering of carbon in carbon-nickel composite thin films. *Carbon* **2007**, *45*, 2995–3006. [[CrossRef](#)]
34. Sedláčková, K.; Lobotka, P.; Vávra, I.; Radnóczy, G. Structural, electrical and magnetic properties of carbon-nickel composite thin films. *Carbon* **2005**, *43*, 2192–2198. [[CrossRef](#)]
35. Babonneau, D.; Briatico, J.; Petroff, F.; Cabioch, T.; Naudon, A. Structural and magnetic properties of Fe<sub>x</sub>C<sub>1-x</sub> nanocomposite thin films. *J. Appl. Phys.* **2000**, *87*, 3432–3443. [[CrossRef](#)]
36. Delli, E.; Baziotti, C.; Pliatsikas, N.; Kalfagiannis, N.; Vourlias, G.; Siozios, A.; Dimitrakopoulos, G.P.; Koutsogeorgis, D.C.; Patsalas, P. Laser-driven structural modifications and diffusion phenomena of plasmonic AlN/Ag stratified films. *Surf. Coat. Technol.* **2016**, *295*, 46–53. [[CrossRef](#)]

